materials

MDPI

Article

Impact of Charge-Trapping Effects on Reliability Instability in $Al_xGa_{1-x}N$/GaN High-Electron-Mobility Transistors with Various Al Compositions

Walid Amir [1], Surajit Chakraborty [1], Hyuk-Min Kwon [2,*] and Tae-Woo Kim [1,*]

[1] Department of Electrical, Electronic and Computer Engineering, University of Ulsan, Ulsan 44610, Republic of Korea
[2] Department of Semiconductor Processing Equipment, Semiconductor Convergence Campus, Korea Polytechnics, Anseong-si 17550, Republic of Korea
* Correspondence: hmkwon@kopo.ac.kr (H.-M.K.); twkim78@ulsan.ac.kr (T.-W.K.)

Abstract: In this study, we present a detailed analysis of trapping characteristics at the $Al_xGa_{1-x}N$/GaN interface of $Al_xGa_{1-x}N$/GaN high-electron-mobility transistors (HEMTs) with reliability assessments, demonstrating how the composition of the Al in the $Al_xGa_{1-x}N$ barrier impacts the performance of the device. Reliability instability assessment in two different $Al_xGa_{1-x}N$/GaN HEMTs [x = 0.25, 0.45] using a single-pulse I_D–V_D characterization technique revealed higher drain-current degradation (ΔI_D) with pulse time for $Al_{0.45}Ga_{0.55}N$/GaN devices which correlates to the fast-transient charge-trapping in the defect sites near the interface of $Al_xGa_{1-x}N$/GaN. Constant voltage stress (CVS) measurement was used to analyze the charge-trapping phenomena of the channel carriers for long-term reliability testing. $Al_{0.45}Ga_{0.55}N$/GaN devices exhibited higher-threshold voltage shifting (ΔV_T) caused by stress electric fields, verifying the interfacial deterioration phenomenon. Defect sites near the interface of the AlGaN barrier responded to the stress electric fields and captured channel electrons—resulting in these charging effects that could be partially reversed using recovery voltages. The quantitative extraction of volume trap density (N_t) using $1/f$ low-frequency noise characterizations unveiled a 40% reduced N_t for the $Al_{0.25}Ga_{0.75}N$/GaN device, further verifying the higher trapping phenomena in the $Al_{0.45}Ga_{0.55}N$ barrier caused by the rougher $Al_{0.45}Ga_{0.55}N$/GaN interface.

Keywords: AlGaN/GaN HEMT; interfacial degradation; fast-transient charge-trapping; pulsed I–V; constant voltage stress (CVS); threshold voltage degradation (ΔV_T); $1/f$ low-frequency noise; volume trap density (N_t)

Citation: Amir, W.; Chakraborty, S.; Kwon, H.-M.; Kim, T.-W. Impact of Charge-Trapping Effects on Reliability Instability in $Al_xGa_{1-x}N$/GaN High-Electron-Mobility Transistors with Various Al Compositions. *Materials* **2023**, *16*, 4469. https://doi.org/10.3390/ma16124469

Academic Editor: Linfeng Lan

Received: 12 May 2023
Revised: 7 June 2023
Accepted: 16 June 2023
Published: 19 June 2023

1. Introduction

High-electron-mobility transistors (HEMTs) based on III-V materials have been the next generation of high-power, high-radio-frequency, and high-temperature devices because of their high carrier concentration, high carrier mobility, and high breakdown voltage [1–3]. GaN-based HEMTs have recently attracted much attention because of their remarkable material properties and device performances, notably in high-power and RF applications up to the sub-terahertz regime [4–6]. These advantageous properties and performances are caused primarily by the excellent quality of the epitaxial layer consisting of the $Al_xGa_{1-x}N$ barrier and the GaN channel layer, resulting from the fundamental electronic properties of two-dimensional electron gas (2DEG) on top of Si, Sapphire, and silicon carbide (SiC) substrates [7–9]. Because high-density 2DEG accumulates at the $Al_xGa_{1-x}N$/GaN interface, those electronic properties would reflect the quality of the interface via scattering procedures caused by dislocations [10]. During device operation, the interface quality of the $Al_xGa_{1-x}N$/GaN is essential for improving carrier transport in the channel [10].

Reliability concerns of $Al_xGa_{1-x}N$/GaN HEMTs have been caused by trap effects related to a drain, gate lag, and current collapse with various types of degradation [11–13]. The AlGaN layer, which is usually the surface layer and has an interface with the GaN channel, is a source of reliability instability, including trapping in the gate-to-drain access region, deep-level, and $Al_xGa_{1-x}N$/GaN interface [14]. Although most surface traps can be passivated with different kinds of passivation layers (e.g., SiN_x, SiO_2, and Al_2O_3), optimization of the traps inside the $Al_xGa_{1-x}N$ layer and the $Al_xGa_{1-x}N$/GaN interface is still an ongoing investigation. The reliability instability issues of the $Al_xGa_{1-x}N$/GaN HEMTs are worse than that of conventional *Si*-based devices because of the interface quality of the $Al_xGa_{1-x}N$/GaN [15–17].

The defect sites in the AlGaN barrier layer and the interface $Al_xGa_{1-x}N$/GaN are the predominant cause of the transient-charging effects (Figure 1) [18,19]. The transient-charging effects follow two different processes, fast and slow transient charging. Channel carriers are easily injected into shallow defects (fast-transient charging) in the $Al_xGa_{1-x}N$ barrier layer and the interface of $Al_xGa_{1-x}N$/GaN. Then, trapped charges in the shallow trap site follow thermally activated electron migration via trap-to-trap conduction (slow transient charging). The fast-transient-charging effect is responsible for mobility degradation and threshold voltage (V_T) instability in AlGaN/GaN HEMTs, while the slow transient charging causes long-term stress V_T instability. All of these are major concerns for implementing GaN-based HEMTs in future applications. Improving the reliability instability of $Al_xGa_{1-x}N$/GaN HEMTs requires thoroughly analyzing the trapping effects because the channel carriers can easily tunnel into the pre-existing defect sites in the $Al_xGa_{1-x}N$ barrier layer and the interface $Al_xGa_{1-x}N$/GaN.

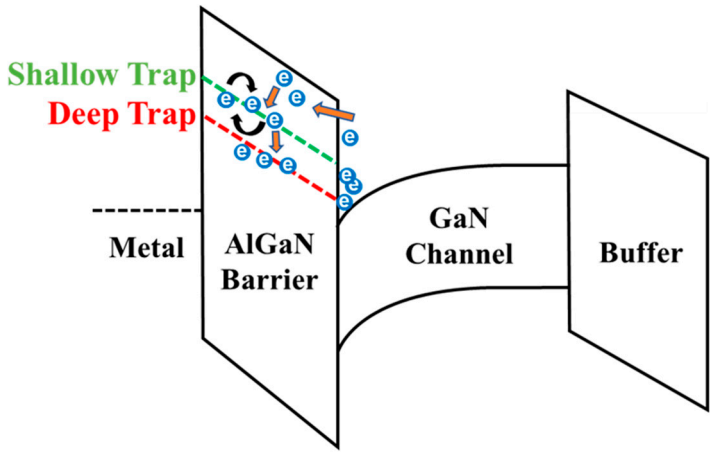

Figure 1. Schematic of the band diagram of $Al_xGa_{1-x}N$/GaN HEMTs defining the "Shallow" and "Deep" trap states that capture tunneling channel carriers.

In this study, a comprehensive analysis of the trapping effects in $Al_xGa_{1-x}N$/GaN HEMTs with varying Al compositions was performed to optimize the device structure to obtain improved performance. We performed a reliability instability assessment in two different $Al_xGa_{1-x}N$/GaN HEMTs [x = 0.25, 0.45] using a single-pulse I_D–V_D technique that could be demonstrated by fast-transient-charging effects. For long-term reliability testing, we performed constant voltage stress (CVS) measurements under high-drain bias conditions to analyze the charge-trapping phenomena of the channel carriers. V_T shifting during constant voltage stress was compared between the devices to verify the interfacial degradation phenomena. Furthermore, the flicker noise characteristics were analyzed to gain knowledge of the dominant defect locations of the two structures. Finally, to verify the quantitative analysis of the trapping effects, the trap density (N_t) of both samples was calculated using the carrier mobility fluctuation (CMF) model [20].

2. Experimental Details

Figure 2 represents the fabrication process flow and the cross-sectional illustration of the $Al_xGa_{1-x}N$/GaN HEMTs used in this study. The epitaxial layers were grown on a semi-insulating SiC substrate using metal-organic chemical vapor deposition (MOCVD). Each layer was grown in the following order: ~270 nm of an AlN buffer layer, ~400 nm of GaN channel, and ~20 nm of an $Al_xGa_{1-x}N$ [x = 0.25, 0.45] barrier layer. Cl_2-based inductively-coupled plasma (ICP) etching was used to isolate the devices for the mesa isolation procedure. The substrate was then cleaned for 30 s with a 1:5 solution of HCl and deionized water to remove any native oxide. The ohmic metallization of the source and drain was performed by an e-beam evaporator with a metal scheme of Ti/Al/Ni/Au (25/160/40/100 nm). Rapid thermal annealing was used to alloy the ohmic contacts at 830 °C and under N_2 ambient for 30 s. An additional padding layer of Ti/Au (20/300 nm) was deposited by an e-beam evaporator to ensure proper probe contact during device characterization. The contact resistance (R_C) and sheet resistance (R_{SH}) from TLM measurements were 0.25 Ω·mm and 380 Ω/□ for the Al = 25% sample and 0.28 Ω·mm and 420 Ω/□ for the Al = 45% sample, respectively. Finally, the gate pattern was defined using e-beam lithography, and a T-shaped Ni/Au (20/400 nm) short-channel gate was deposited. Gate-source and gate-drain distances were kept symmetrical, and the drain-to-source distance was fixed at 2 µm. All electrical characteristics were analyzed using the Keysight B1500A semiconductor parameter analyzer. The fast-transient-charging effect characterization was conducted using the single-pulse I_D–V_D with a pair of B1530A waveform generator modules. For the *1/f* low-frequency flicker noise measurements, we used a dynamic signal analyzer HP 35670A and a current preamplifier SR570.

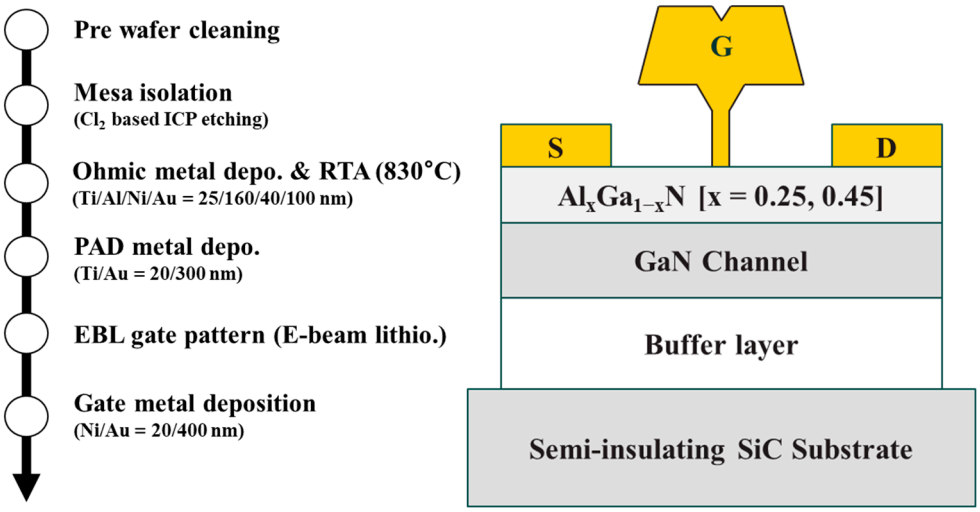

Figure 2. Fabrication process flow and the cross-section illustration of the $Al_xGa_{1-x}N$/GaN HEMTs with different Al [25%, 45%] compositions in the barrier layer.

3. Results and Discussion

3.1. Charge-Trapping Analysis with Pulsed I–V

Figure 3a shows the DC transfer characteristics comparison of the devices with respect to the gate overdrive voltage (V_{GS}–V_T). Although the device characteristics are quite similar in DC measurements, the Al = 25% sample showed slightly higher drain current I_D (at high V_{GS}–V_T) and transconductance G_m. Figure 3b illustrates single-pulse I_D-V_D characteristics with different Al compositions in the barrier layer. The output characteristics of a single-pulse I_D–V_D technique with the rise (t_r) and fall time (t_f) of 50 ns were measured with a V_D sweep. Rise and fall times were kept small to achieve trap-free I_D–V_D characteristics [21]. A short pulse width of the gate and drain was applied during the measurement, reducing fast-transient trapping/de-trapping effects.

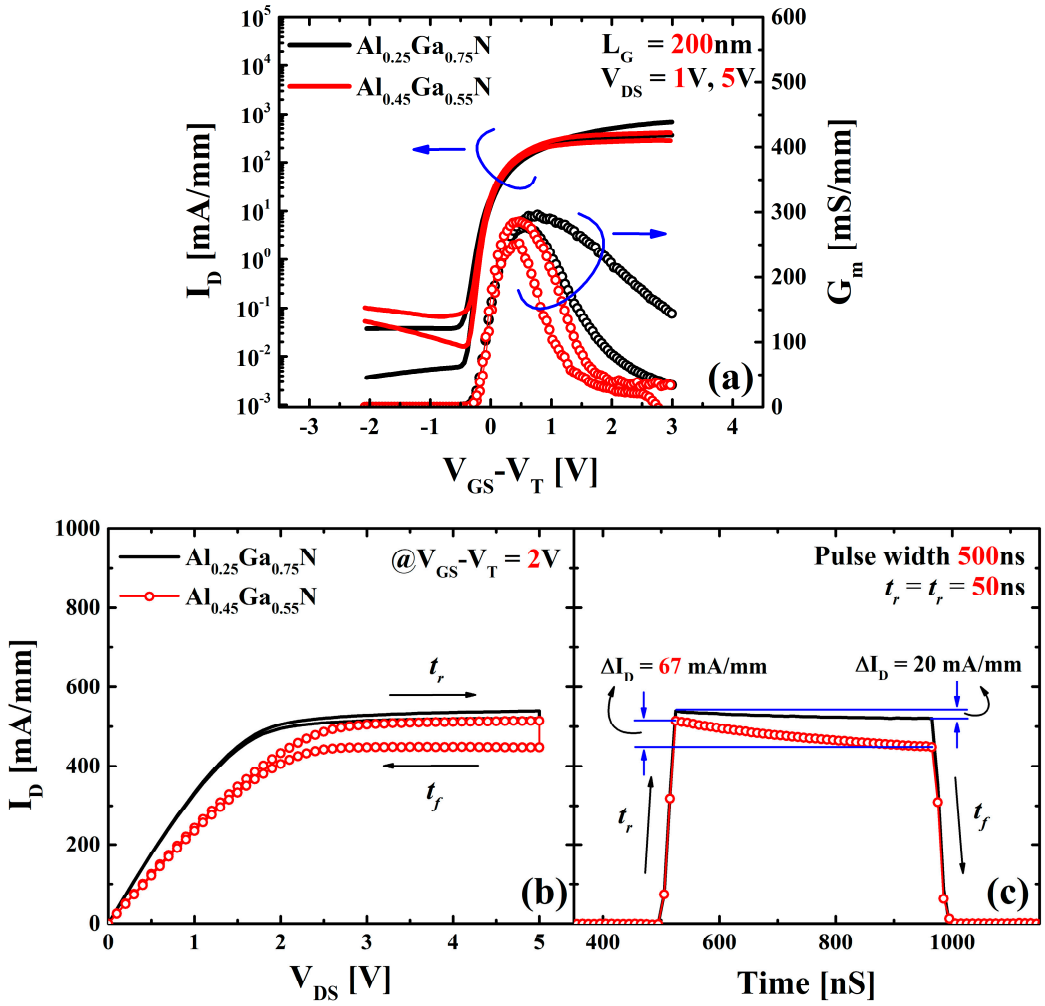

Figure 3. (**a**) DC transfer characteristics of the samples at V_{DS} = 1, 5 V with respect to the gate overdrive voltage (V_{GS}–V_T). (**b**) A single-pulse I_D–V_D characteristics of AlGaN/GaN HEMTs with different Al compositions. (**c**) Rapid deterioration of the drain current over time when a maximum pulse is applied to both gate and drain, which is consistent with the pulsed I_D–V_D sweep.

A significant reduction in the drain-current (ΔI_D) is observed during the fall-down trace for the Al = 45% sample compared with the Al = 25% sample, related to the filling of the resonant traps during the rise time and pulse width through the fast-transient charging process. DC measurements cause a significant degradation because of higher integration time (~5 ms) [22,23].

Figure 3c depicts the fast degradation in the drain-current with respect to time when the gate pulse is V_{GS}–V_T = 2 V and drain bias is V_{DS} = 5 V, corresponding to the pulsed I_D-V_D characteristics. Channel carriers are trapped in the trap states near the interface of the $Al_xGa_{1-x}N$ barrier layer and the interface $Al_xGa_{1-x}N$/GaN [23,24]. I_D degradation for $Al_{0.25}Ga_{0.75}N$/GaN device during 500 ns pulse width is ~20 mA/mm, while $Al_{0.45}Ga_{0.55}N$/GaN device illustrates I_D degradation in ~67 mA/mm. A significantly higher I_D degradation for the Al = 45% sample corresponds to a rougher interface between the barrier and GaN channel caused by higher lattice mismatching.

Drain-current degradation with respect to pulsed time is related to charge-trapping in the defect sites, which can be explained by the model of charging processes [25]. Channel carriers can be tunneled into the shallow defect sites in the AlGaN barrier layer and can occur to thermally activated electron migration between the defect sites with temperature dependency. The location of these defect sites is below the conduction band, as illustrated in Figure 1. Because of the extremely low trap energy of these shallow traps and the high

density of states (DOE) from the GaN conduction band, the charging process will have a fast charging time. Slow transient charging can be attributed to the capture of secondary electrons induced from the trapped charges from the fast charging process.

3.2. Charge-Trapping Analysis with Constant Voltage Stress Condition

A long-term reliability evaluation was performed under high electric field conditions to verify the interfacial degradation from charge-trapping. Figure 4a illustrates the charge-trapping and de-trapping characteristics of two samples during a complete cycle of constant voltage stress at both gate and drain and relaxation cycle. Applied stress conditions were V_{GS} = 2 V and V_{DS} = 5 V. Threshold voltage shifting (ΔV_T) from trapping in the interface states was evident. Channel carriers are trapped in the defect sites of the $Al_xGa_{1-x}N$ barrier via the interface caused by a high electric field and thin barrier layer [24,26]. The degradation in V_T is consistent with the electron trapping at the $Al_xGa_{1-x}N$ barrier layer defect locations from the GaN channel layer. This trapping phenomenon can be partially recovered by applying recovery voltages of V_{GS} and V_{DS} = 0 V.

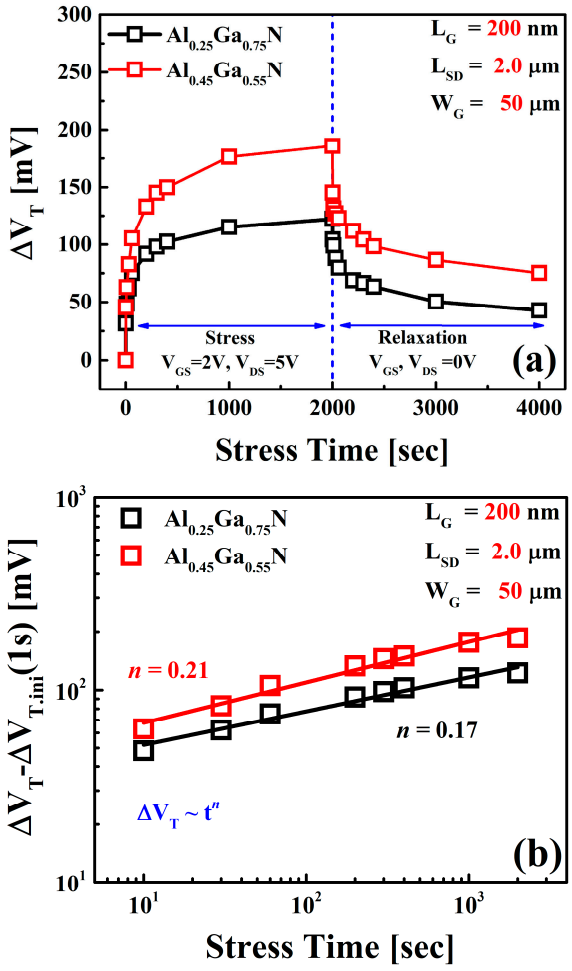

Figure 4. (**a**) Threshold voltage shift (ΔV_T) characteristics of AlGaN/GaN HEMTs during constant voltage stress at high drain bias (V_{DS} = 5 V) condition illustrating charge-trapping and de-trapping properties of the channel electrons. (**b**) Power-law time dependency of the observed ΔV_T excluding the fast-transient charge-trapping components ($\Delta V_T - \Delta V_{T.initial\ (1\ s)}$) in two samples.

The fast-transient trapping effect, which is active during a short (<1 ms), is accountable for the substantial change in the initial V_T (1 s). This effect is caused by the tunneling of channel carriers in the pre-existing defect sites inside the $Al_xGa_{1-x}N$ barrier. The ΔV_T characteristics at Al = 45% had a higher initial ΔV_T and more degradation than at Al = 25%.

The time dependence of the V_T was investigated to quantify the charge-trapping phenomenon (Figure 4b). The fast-transient charge-trapping component, which is supposed to saturate fully after 1 s of stress, may be eliminated, and the power-law equation can be used to describe the time dependence $\Delta V_T \sim t^n$ of the ΔV_T ($\Delta V_T - \Delta V_{T.initial}$ (1 s)) [23,27,28]. Both devices degrade according to the power-law kinetics. Time exponent, n, is in the range of 0.17–0.21, a similar but somewhat lower range than for the Al = 25% device, corresponding to a lower interfacial degradation [29]. Regardless of the value of n, the ΔV_T values of Al = 45% devices are much higher than the Al = 25% device associated with higher trap states in the $Al_{0.45}Ga_{0.55}N$ barrier.

3.3. Quantitative Analysis of Trap Density with 1/f Low-Frequency Noise

Low-frequency noise (LFN) is an effective tool for analyzing the interface states in a semiconductor device—predominantly responsible for performance degradation. A flicker noise(*1/f* noise) is usually generated from the following two causes: Carrier Number Fluctuation (CNF) and Carrier Mobility Fluctuation (CMF) [20]. Both are related to charge-trapping from the channel to the gate dielectric or barrier layer. Carrier interaction between the channel and the near-interface dielectric/barrier traps causes CNF noise. These charging effects also cause fluctuation in carrier mobility and result in correlated mobility fluctuations [30,31]. Both CNF and CMF should be considered for the quantitative trap extraction to evaluate accurate charge-trapping phenomena. With the CMF model proposed in the literature [20], it is possible to gain knowledge on the *1/f* noise in all the operation regions (from linear to saturation and weak to strong inversion).

The *1/f* noise measurements were performed from 1 Hz to 10 kHz at a fixed drain bias of V_{DS} = 0.5 V from off-state to accumulation, including the linear region. Figure 5a illustrates the normalized power spectral density ($S_{ID}/I_D{}^2$) with respect to the frequency at $V_{GS} = V_T$ condition. The power-law equation ($1/f^{\gamma}$ function) is used to explain the frequency dependency of power spectral density (PSD) [18]. The $1/f^{\gamma}$ function was fitted with the measured data over the frequency range of 1 Hz to 10 kHz to extract the value of the frequency component (γ) [19]. Based on Table 1, the value of γ is in the range of 1–1.3 (near 1), indicating that the defects/traps had uniform depth and energy [32]. Al = 45% devices had a γ value of 1.3 (Over 1), indicating that the most dominant trap locations are close to the interface of the $Al_{0.45}Ga_{0.55}N$ barrier and GaN channel.

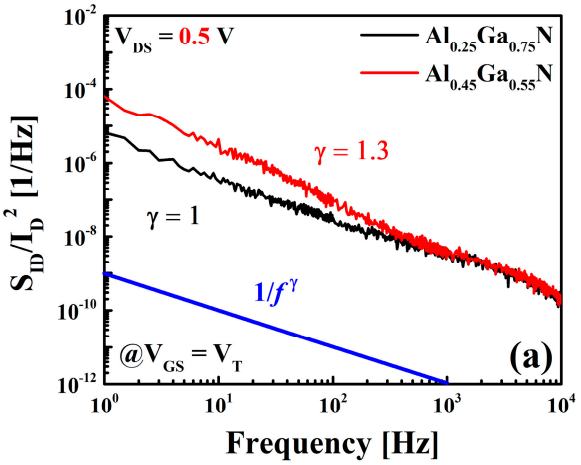

Figure 5. *Cont.*

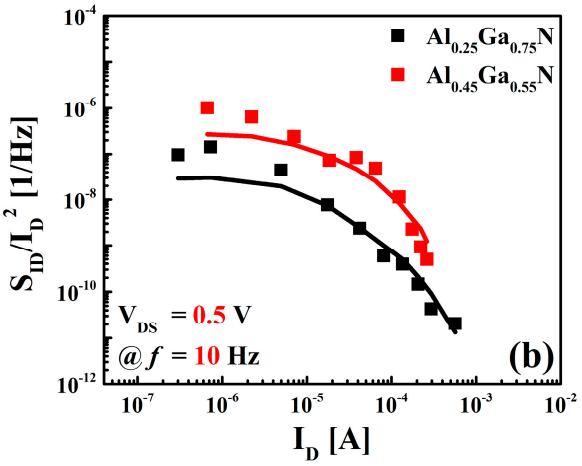

Figure 5. (**a**) Comparison of the normalized drain-current power spectral density (PSD) ($S_{ID}/I_D{}^2$) at $V_{GS} = V_T$ and V_{DS} = 0.5 V. The frequency component (γ) is in the range of 1~1.3. (**b**) Fitting curves of $S_{ID}/I_D{}^2$ values using the CMF model calculated at a frequency of 10 Hz.

Table 1. Comparison of the key reliability parameters of the AlGaN/GaN HEMTs.

Sample	ΔI_D [mA/mm]	n	γ	N_t [$cm^{-3}{\cdot}eV^{-1}$]
$Al_{0.25}Ga_{0.75}N/GaN$	20	0.17	1	1.8×10^{19}
$Al_{0.45}Ga_{0.55}N/GaN$	67	0.21	1.3	3×10^{19}

For the quantitative analysis of the trap states, the trap density (N_t) was extracted using the CMF model, as represented by [20,31]:

$$\frac{S_{ID}}{I_D^2} = \left(\frac{G_m}{I_D}\right)^2 \left(1 + \alpha_{SC}\mu_{eff}C_B\frac{I_D}{G_m}\right)^2 S_{Vfb} \quad (1)$$

where the variable α_{sc} is the coefficient for Coulomb scattering, μ_{eff} is the effective mobility of the carriers, and C_B is the capacitance per unit area of the AlGaN barrier. S_{Vfb} is the flat-band voltage and can be defined as follows [33–35]:

$$S_{Vfb} = \frac{q^2kT\lambda N_t}{WLC_B^2 f} \quad (2)$$

where q, kT, and N_t are symbols used to represent elemental charge, thermal energy, and trap density, respectively. $\lambda = [4\pi(2m^*\Phi_B)^{1/2}/h]^{-1}$ represents the attenuation tunneling distance (Φ_B denotes the barrier height) [36]. Figure 5b illustrates a good fitting between the normalized drain-current power spectral density ($S_{ID}/I_D{}^2$) and the right side of Equation (1), which prevails in the CMF model. Using Equation (2) and the S_{Vfb} extracted from the fitting, N_t for both devices was extracted. Al = 45% devices had a 40% higher N_t value of 3×10^{19} $cm^{-3}{\cdot}eV^{-1}$ compared with 1.8×10^{19} $cm^{-3}{\cdot}eV^{-1}$ for the Al = 25% devices. The reason for these noise characteristics is attributed to the fact that the $Al_{0.45}Ga_{0.55}N/GaN$ interface creates higher defect sites near the interface, which increases the probability of the channel electron tunneling into the AlGaN barrier layer.

4. Conclusions

We demonstrated an in-depth trapping characteristic analysis of the $Al_xGa_{1-x}N/GaN$ interface of AlGaN/GaN HEMTs based on the Al composition in the $Al_xGa_{1-x}N$ barrier and how it affects device performance. Higher I_D degradation for the $Al_{0.45}Ga_{0.55}N/GaN$ devices during the pulsed I_D-V_D characterization was attributed to the higher fast-transient

trapping in the $Al_{0.45}Ga_{0.55}N$/GaN interface and reliability instability. During constant voltage stress conditions, the $Al_{0.45}Ga_{0.55}N$/GaN device had a higher V_T shift corresponding to higher trapping in the $Al_{0.45}Ga_{0.55}N$ barrier. A larger time exponent n in the $Al_{0.45}Ga_{0.55}N$/GaN device indicated higher interfacial degradation. During quantitative extraction of volume trap density, the $Al_{0.45}Ga_{0.55}N$/GaN device had a 40% higher N_t, further verifying the higher trapping phenomena in the $Al_{0.45}Ga_{0.55}N$ barrier caused by the rougher $Al_{0.45}Ga_{0.55}N$/GaN interface. These results demonstrate that trapping effects, which impact device performance considerably, are influenced primarily by the quality of the interface between the AlGaN and GaN layers. Future applications of the GaN HEMT devices can benefit from enhanced device properties by lowering the Al content to reduce lattice mismatches.

Author Contributions: T.-W.K. and W.A. generated the main concept of this work. W.A. conducted most of the experiments and wrote the original manuscript, including preparing figures and electrical characterizations; S.C. helped in the formal analysis; H.-M.K. supervised the work and reviewed the manuscript; T.-W.K. initiated this study and supervised the entire process. All authors analyzed and discussed the results. All authors have read and agreed to the published version of the manuscript.

Funding: This work was supported by the 2022 Research Fund of the University of Ulsan.

Data Availability Statement: The data presented in this study are available on request from the corresponding author.

Conflicts of Interest: The authors declare no conflict of interest.

References

1. Del Alamo, J.A. Nanometre-Scale Electronics with III–V Compound Semiconductors. *Nature* **2011**, *479*, 317–323. [CrossRef] [PubMed]
2. Baek, J.-M.; Kim, H.-J.; Yoo, J.-H.; Shin, J.-W.; Shin, K.-Y.; Amir, W.; Ju, G.; Kim, H.-J.; Oh, J.; Kim, H.; et al. Vertical Homo-Junction In0.53Ga0.47As Tunneling Field-Effect Transistors with Minimum Subthreshold Swing of 52 MV/Decade. *Solid-State Electron.* **2022**, *197*, 108447. [CrossRef]
3. Shin, K.Y.; Shin, J.W.; Chakraborty, S.; Amir, W.; Shin, C.S.; Kim, T.W. Trap Behavior of Metamorphic HEMTs with Pulsed IV and 1/f Noise Measurement. In Proceedings of the European Solid-State Device Research Conference, Milan, Italy, 19–22 September 2022; Volume 2022, pp. 324–327. [CrossRef]
4. Sheppard, S.T.; Doverspike, K.; Pribble, W.L.; Allen, S.T.; Palmour, J.W.; Kehias, L.T.; Jenkins, T.J. High-Power Microwave GaN /AlGaN HEMT's on Semi-Insulating Silicon Carbide Substrates. *IEEE Electron Device Lett.* **1999**, *20*, 161–163. [CrossRef]
5. Brown, D.F.; Williams, A.; Shinohara, K.; Kurdoghlian, A.; Milosavljevic, I.; Hashimoto, P.; Grabar, R.; Burnham, S.; Butler, C.; Willadsen, P.; et al. W-Band Power Performance of AlGaN/GaN DHFETs with Regrown N+ GaN Ohmic Contacts by MBE. In Proceedings of the IEEE International Electron Devices Meeting (IEDM), Washington, DC, USA, 5–7 December 2011; pp. 461–464. [CrossRef]
6. Shinohara, K.; Milosavljevic, I.; Burnham, S.; Cornon, A.; Hashimoto, P.; Wong, D.; Hu, M.; Butler, C.; Schmitz, A.; Willadsen, P.J.; et al. 60-Nm GaN/AlGaN DH-HEMTs with 1.0 Ω·mm Ron, 2.0 A/Mm Idmax, and 153 GHz FT. In Proceedings of the Device Research Conference—Conference Digest, DRC, University Park, PA, USA, 22–24 June 2009; pp. 167–168.
7. Shi, J.; Eastman, L.F.; Xin, X.; Pophristic, M. High Performance AlGaN/GaN Power Switch with HfO2 Insulation. *Appl. Phys. Lett.* **2009**, *95*, 7–10. [CrossRef]
8. Liu, Z.H.; Ng, G.I.; Arulkumaran, S.; Maung, Y.K.T.; Teo, K.L.; Foo, S.C.; Sahmuganathan, V. Improved Linearity for Low-Noise Applications in 0.25-Mm GaN MISHEMTs Using ALD Al_2O_3 as Gate Dielectric. *IEEE Electron Device Lett.* **2010**, *31*, 803–805. [CrossRef]
9. Chakraborty, S.; Kim, T.W. Comprehensive Schottky Barrier Height Behavior and Reliability Instability with Ni/Au and Pt/Ti/Pt/Au on AlGaN/GaN High-Electron-Mobility Transistors. *Micromachines* **2022**, *13*, 84. [CrossRef]
10. Mimila-Arroyo, J.; Jomard, F.; Chevallier, J. Improvement of AlGaN/GaN/Si High Electron Mobility Heterostructure Performance by Hydrogenation. *Appl. Phys. Lett.* **2013**, *102*, 092104. [CrossRef]
11. Amir, W.; Shin, J.W.; Chakraborty, S.; Shin, K.Y.; Hoshi, T.; Tsutsumi, T.; Sugiyama, H.; Kwon, H.M.; Kim, T.W. Instability Assessment of AlGaN/GaN High Electron Mobility Transistors Under High Drain Current Condition. In Proceedings of the Asia-Pacific Microwave Conference (APMC 2022), Yokohama, Japan, 29 November–2 December 2022; pp. 184–186. [CrossRef]
12. Chakraborty, S.; Amir, W.; Shin, J.W.; Shin, K.Y.; Cho, C.Y.; Kim, J.M.; Hoshi, T.; Tsutsumi, T.; Sugiyama, H.; Matsuzaki, H.; et al. Explicit Thermal Resistance Model of Self-Heating Effects of AlGaN/GaN HEMTs with Linear and Non-Linear Thermal Conductivity. *Materials* **2022**, *15*, 8415. [CrossRef]

13. Chakraborty, S.; Shin, J.W.; Amir, W.; Shin, K.Y.; Kim, T.W. An Explicit Thermal Resistance Model Regarding Self-Heating Effect of AlGaN/GaN High Electron Mobility Transistor. *Mater. Sci. Forum* **2022**, *1074*, 125–131. [CrossRef]
14. Rossetto, I.; Meneghini, M.; Tajalli, A.; Dalcanale, S.; De Santi, C.; Moens, P.; Banerjee, A.; Zanoni, E.; Meneghesso, G. Evidence of Hot-Electron Effects during Hard Switching of AlGaN/GaN HEMTs. *IEEE Trans. Electron Devices* **2017**, *64*, 3734–3739. [CrossRef]
15. Duan, M.; Zhang, J.F.; Ji, Z.; Zhang, W.; Kaczer, B.; De Gendt, S.; Groeseneken, G. Defect Loss: A New Concept for Reliability of MOSFETs. *IEEE Electron Device Lett.* **2012**, *33*, 480–482. [CrossRef]
16. Chaudhry, A.; Kumar, M.J. Controlling Short-Channel Effects in Deep-Submicron SOI MOSFETs for Improved Reliability: A Review. *IEEE Trans. Device Mater. Reliab.* **2004**, *4*, 99–109. [CrossRef]
17. Amir, W.; Kim, D.H.; Kim, T.W. Comprehensive Analysis of Quantum Mechanical Effects of Interface Trap and Border Trap Densities of High-k $Al_2O_3/In_{0.53}Ga_{0.47}As$ on a 300-Mm Si Substrate. *IEEE Access* **2020**, *8*, 211464–211473. [CrossRef]
18. Kwon, H.M.; Kim, D.H.; Kim, T.W. Impact of Fast and Slow Transient Charging Effect on Reliability Instability in In0.7Ga0.3As Quantum-Well MOSFETs with High-κ Dielectrics. *Jpn. J. Appl. Phys.* **2020**, *59*, 110903. [CrossRef]
19. Amir, W.; Shin, J.; Shin, K.; Chakraborty, S.; Cho, C.; Kim, J.; Lee, S.; Hoshi, T.; Tsutsumi, T.; Sugiyama, H.; et al. Performance Enhancement of AlGaN/GaN HEMT via Trap-State Improvement. *IEEE Trans. Electron Devices* **2023**, *170*, 2988–2993. [CrossRef]
20. Ioannidis, E.G.; Dimitriadis, C.A.; Haendler, S.; Bianchi, R.A.; Jomaah, J.; Ghibaudo, G. Improved Analysis and Modeling of Low-Frequency Noise in Nanoscale MOSFETs. *Solid-State Electron.* **2012**, *76*, 54–59. [CrossRef]
21. Young, C.D.; Zhao, Y.; Heh, D.; Choi, R.; Lee, B.H.; Bersuker, G. Pulsed Id-Vg Methodology and Its Application to Electron-Trapping Characterization and Defect Density Profiling. *IEEE Trans. Electron Devices* **2009**, *56*, 1322–1329. [CrossRef]
22. Bersuker, G.; Zeitzoff, P.; Sim, J.H.; Lee, B.H.; Choi, R.; Brown, G.; Young, C.D. Mobility Evaluation in Transistors with Charge-Trapping Gate Dielectrics. *Appl. Phys. Lett.* **2005**, *87*, 2003–2006. [CrossRef]
23. Heh, D.; Young, C.D.; Choi, R.; Bersuker, G. Extraction of the Threshold-Voltage Shift by the Single-Pulse Technique. *IEEE Electron Device Lett.* **2007**, *28*, 734–736. [CrossRef]
24. Heh, D.; Young, C.D.; Brown, G.A.; Hung, P.Y.; Diebold, A.; Bersuker, G.; Vogel, E.M.; Bernstein, J.B. Spatial Distributions of Trapping Centers in HfO_2/SiO_2 Gate Stacks. *Appl. Phys. Lett.* **2006**, *88*, 152907. [CrossRef]
25. Bersuker, G.; Sim, J.H.; Park, C.S.; Young, C.D.; Nadkarni, S.V.; Choi, R.; Lee, B.H. Mechanism of Electron Trapping and Characteristics of Traps in HfO_2 Gate Stacks. *IEEE Trans. Device Mater. Reliab.* **2007**, *7*, 138–145. [CrossRef]
26. Bersuker, G.; Park, C.S.; Barnett, J.; Lysaght, P.S.; Kirsch, P.D.; Young, C.D.; Choi, R.; Lee, B.H.; Foran, B.; Van Benthem, K.; et al. The Effect of Interfacial Layer Properties on the Performance of Hf-Based Gate Stack Devices. *J. Appl. Phys.* **2006**, *100*, 094108. [CrossRef]
27. Young, C.D.; Zeitzoff, P.; Brown, G.A.; Bersuker, G.; Lee, B.H.; Hauser, J.R. Intrinsic Mobility Evaluation of High-K Gate Dielectric Transistors Using Pulsed Id-Vg. *IEEE Electron Device Lett.* **2005**, *26*, 586–589. [CrossRef]
28. Young, C.D.; Heh, D.; Neugroschel, A.; Choi, R.; Lee, B.H.; Bersuker, G. Electrical Characterization and Analysis Techniques for the High-κ Era. *Microelectron. Reliab.* **2007**, *47*, 479–488. [CrossRef]
29. Cho, M.; Lee, J.D.; Aoulaiche, M.; Kaczer, B.; Roussel, P.; Kauerauf, T.; Degraeve, R.; Franco, J.; Ragnarsson, L.Å.; Groeseneken, G. Insight into N/PBTI Mechanisms in Sub-1-Nm-EOT Devices. *IEEE Trans. Electron Devices* **2012**, *59*, 2042–2048. [CrossRef]
30. Hung, K.K.; Ko, P.K.; Hu, C.; Cheng, Y.C. A Unified Model for The Flicker Noise In Metal-Oxide-Semiconductor Field-Effect Transistors. *IEEE Trans. Electron Devices* **1990**, *37*, 654–665. [CrossRef]
31. Ghibaudo, G.; Roux, O.; Nguyen-Duc, C.; Balestra, F.; Brini, J. Improved Analysis of Low Frequency Noise in Field-Effect MOS Transistors. *Phys. Status Solidi* **1991**, *124*, 571–581. [CrossRef]
32. Han, I.S.; Kwon, H.M.; Bok, J.D.; Kwon, S.K.; Jung, Y.J.; Choi, W.I.; Choi, D.S.; Lim, M.G.; Chung, Y.S.; Lee, J.H.; et al. Effect of Nitrogen Concentration on Low-Frequency Noise and Negative Bias Temperature Instability of p-Channel Metal-Oxide-Semiconductor Field-Effect Transistors with Nitrided Gate Oxide. *Jpn. J. Appl. Phys.* **2011**, *50*, 12–16. [CrossRef]
33. Amir, W.; Shin, J.W.; Shin, K.Y.; Kim, J.M.; Cho, C.Y.; Park, K.H.; Hoshi, T.; Tsutsumi, T.; Sugiyama, H.; Matsuzaki, H.; et al. A Quantitative Approach for Trap Analysis between Al0.25Ga0.75N and GaN in High Electron Mobility Transistors. *Sci. Rep.* **2021**, *11*, 22401. [CrossRef]
34. Nanowire, G.; Bae, Y.; Ghibaudo, G.; Cristoloveanu, S. 1/f-Noise in AlGaN/GaN Nanowire Omega-FinFETs. *IEEE Electron Device Lett.* **2017**, *38*, 252–254.
35. Vodapally, S.; Theodorou, C.G.; Bae, Y.; Ghibaudo, G.; Cristoloveanu, S.; Im, K.-S.; Lee, J. Comparison for 1/f Noise Characteristics of AlGaN/GaN FinFET and Planar MISHFET. *IEEE Trans. Electron Devices* **2017**, *64*, 3634–3638. [CrossRef]
36. Yin, R.; Li, Y.; Sun, Y.; Wen, C.P.; Hao, Y.; Wang, M. Correlation between Border Traps and Exposed Surface Properties in Gate Recessed Normally-off Al2O3/GaN MOSFET. *Appl. Phys. Lett.* **2018**, *112*, 2–7. [CrossRef]